PCCP

Accepted Manuscript

ROYAL SOCIETY OF CHEMISTRY

www.rsc.org/pccp

Journal Name

ARTICLE

Mechanism of Action of Ethylene Sulfite and Vinylene Carbonate Electrolyte Additives in $LiNi_{1/3}Mn_{1/3}Co_{1/3}O_2$/graphite Pouch Cells: Electrochemical, GC-MS and XPS analysis.

Received 00th January 20xx,
Accepted 00th January 20xx

DOI: 10.1039/x0xx00000x

www.rsc.org/

L. Madec[a], R. Petibon[b], K. Tasaki[c], J. Xia[a], J.-P. Sun[a], I. G. Hill[a] and J. R. Dahn[a,b,*]

The role of ethylene sulfite used either alone or in combination with VC in $LiNi_{1/3}Mn_{1/3}Co_{1/3}O_2$ (NMC)/graphite pouch cells was studied by correlating data from differential capacity (d*Q*/d*V*) analysis, gas chromatography/mass spectroscopy (GC–MS), theoretical calculations, ultrahigh precision coulometry, storage experiments and X-ray photoelectron spectroscopy. For cells containing VC alone, the electrochemical performance and gas production were greatly improved, compared to cells without VC, due to the formation of more stable and protective SEI films at both electrode surfaces by a polymer of VC. For cells with ES alone, a vigorous reactivity was observed due to preferential reduction that also generated large amounts of gas during formation. The dramatic decrease in electrochemical performance as well as the continuous production of gas during cycling in cells with ES was explained by the formation of a very thin and ineffective SEI film at the NMC surface. The suppression of the vigorous reaction of ES in cells with both ES and VC occurred because the solvation energy of Li^+ by VC is smaller than that of EC so VC is reduced first during formation. During charge-discharge cycling, a slow consumption of ES occurred and different sulfur species were observed on the electrodes when VC was combined with ES. SEI film formation processes and SEI composition were therefore dominated by VC and the electrochemical performance of cells with both VC and ES were similar compared to those of cells with VC alone.

1. Introduction

Extending the life time of Li-ion cells to several decades, for vehicle and grid storage applications, is one of the most challenging problems for battery researchers. The main factor that impacts the cell lifetime of Li-ion cells is the degradation of electrolyte solvents and/or salts that can occur during cycling and storage. The degradation results in the formation of very complex organic- and inorganic-based surface films at the electrolyte/electrode interfaces, referred to as the solid electrolyte interphases (SEI).[1] To address this issue, electrolyte additives are commonly used as a simple, economical and effective approach to improve both cycle and calendar life as well as the rate capability of Li-ion batteries.[2,3] The main role of electrolyte additives is therefore to prevent or hinder such unwanted parasitic reactions by modifying the SEI films. Although the chemical nature and morphology of those films have been carefully analysed during the last decade, most studies have been on common electrolytes with no additives (e.g. a mixture of carbonate solvents with $LiPF_6$ as the salt). Therefore, despite increasing numbers of studies on electrolyte additives, their exact impact on the chemistry and morphology of the SEI still remain poorly understood.

Vinylene carbonate or 1,3-Dioxol-2-one (VC, Figure 1) is probably the most used and known electrolyte additive for Li-ion cells[4,5,6,7] since the time it was proposed by SAFT.[8] VC has been found to improve the electrochemical performance and thermal stability of different Li-ion systems[9,10,11,12,13]. In addition to the beneficial impact of VC on the negative electrode, VC has also been shown to cause major beneficial effects on positive electrodes.[5,7,10,12] For instance, high precision coulometry[14] and storage experiments[15] have recently shown that VC decreases the rate of electrolyte oxidation at the positive $LiCoO_2$ [16] and $LiNi_{1/3}Mn_{1/3}Co_{1/3}O_2$ [17] electrodes. Performance degradation and/or gas evolution of VC-containing cells appear, however, at very high volatges[18] and high temperatures[19] due to extensive electrolyte degradation. The reactivity of VC is greatly influenced by its polymerizable vinyl group. So far, various mechanisms have been proposed to explain the formation of different VC polymerization products as well as nonpolymeric species.[5,20,21] Based on XPS analysis and theoretical simulations, Ouatani *et*

[a] *Department of Physics and Atmospheric Science, Dalhousie University, Halifax, B3H4R2, Canada.*
[b] *Department of Chemistry, Dalhousie University, Halifax, B3H4R2, Canada.*
[c] *Mitsubishi Chemical USA, Redondo Beach, California, USA.*
* Corresponding author: jeff.dahn@dal.ca

† Electronic Supplementary Information (ESI) available: [Materials and methods. SEM images of the top surface of the NMC and graphite electrodes taken from a dry pouch cell. Picture of the gas extraction device designed for the extraction of gaseous components of Li-ion pouch cells. Pictures of the transfer system used to transfer moisture/air sensitive electrode samples from the argon-filled glovebox to the XPS spectrometer. Cu 2p XPS core spectrum of the graphite electrode after formation with 2% ES electrolyte. Enlarged C 1s and O 1s XPS core spectra for graphite electrodes and enlarged O 1s XPS core spectra for NMC electrodes for the different electrolytes. Atomic percentage (at. %) of the P 2p peaks associated with phosphates and fluorophosphates measured at the surface of graphite and NMC electrodes]. See DOI: 10.1039/x0xx00000x

al.[22] have, however, found that a radical polymerization mechanism of VC is more likely the main reaction pathway at the surface of both electrodes of a $LiCoO_2$/graphite cell. They also proved that during the reaction of VC, no interaction occurred between the negative and positive electrodes (e.g. exchange of chemical species from one electrode to the other) as during the first charge of a $LiFePO_4$/graphite cell, the polymeric product of VC was found only at the surface of the graphite[23] while it is observed at both electrodes for a $LiCoO_2$/graphite cell[22]. More recently, Madec *et al*. [24] also reported the formation of an oligomer of VC at the surface of both electrodes of $LiNi_{1/3}Mn_{1/3}Co_{1/3}O_2$(NMC)/graphite pouch cells when VC was used either alone or in combination with a sulfate additive.

Sulfur-containing compounds have also been proposed as SEI film forming electrolyte additives with promising performance.[25,26,27,28,29] Ethylene sulfite or 1,3,2-Dioxathiolan-2-oxide (ES, Figure 1) has been widely used as film forming additive to prevent and even suppress exfoliation of graphite in propylene carbonate (PC) based electrolytes.[30,31,32,33,34,35] Based on theoretical calculations, Xing *et al*.[36] proposed a one-electron reduction mechanism of ES in PC-containing electrolyte with $LiOSO_2$ and $ROSO_2Li$ as the main species formed on the SEI film at the graphite electrode. Leggesse *et al*.[37] also investigated the reductive decomposition of ES in PC-based electrolyte with a theoretical approach. They suggested that ES can react through both one- and two-electron reduction to give $(CH_2OSO_2Li)_2$, other $ROSO_2Li$ species, $CH_3CH(OSO_2Li)CH_2OCO_2Li$ and Li_2SO_3 as major products with inorganic products being more favorably formed in the two-electron reaction pathway. Bhatt *et al*.[38] also showed that in PC electrolyte, from both the first and second electron reduction energies, ES is preferentially reduced compared to VC. A study by Ota *et al*.[39] reports an experimental analysis of the sulfur component formed on both electrodes of graphite/$LiCoO_2$ cells with ES as additive in PC solvent by using X-ray absorption fine structure (XAFS), X-ray photoelectron spectroscopy (XPS) and time-of-flight–secondary ion mass spectrometry (TOF–SIMS). By comparison with standard sulfur compounds, they found that the SEI film on graphite contained mainly sulfite compounds such as inorganic Li_2SO_3, organic $ROSO_2Li$ as well as some organic alkyl sulfide species such as R-S-S-R and/or R-S-R while for the $LiCoO_2$ electrodes, only alkyl sulfide species were present. More recently, Xia *et al*.[40] studied the effect of ES either singly or in combination with VC on $LiNi_{1/3}Mn_{1/3}Co_{1/3}$(NMC)/graphite pouch cells. Using storage experiments and Ultra High Precision Coulometry (UHPC)[41,42] they showed that ES used alone is not a competitive additive due to extensive voltage drop during storage and large charge end point capacity slippage during cycling that results in high coulombic inefficiency (1 – coulombic efficiency = CIE). Significant gas formation during cycling as well as impedance increase were main issues for long term cycling. However, when ES was combined with VC, they found a similar CIE, charge end point capacity slippage and voltage drop as 2% VC used singly with several benefits to the cell performance, such as virtually no gas production during formation and cycling as well as greatly lower impedance of the cell after cycling (by about 50%) mainly due to the graphite electrode contribution. They concluded that VC stabilizes the issues arising from ES at the NMC electrode while ES reduces the high impedance created by VC at the graphite electrode.

In the present study, the role of ES additives used singly or in combination with VC on the electrochemical performances and the resulting lifetime of $LiNi_{1/3}Mn_{1/3}Co_{1/3}O_2$(NMC)/graphite pouch cells has been investigated. Gas chromatography coupled with electron impact mass spectroscopy (GC-MS) measurements have been performed to follow the consumption of the additives and understand the dQ/dV *vs. V* plots recorded during the early stages of the formation cycle. Theoretical calculations were used to investigate the reactivity of ES and VC alone or in combination and the results were used to understand the experimental reactivity observed from the dQ/dV plots. GC-MS was also used to analyze the different gases generated in the pouch cells with the different electrolytes during the formation cycle. Ultra high precision coulometry and storage experiments have been performed to highlight the differences of CIE, charge end point capacity slippage and voltage drop during storage between the different electrolytes. SEI films formed at the surface of both negative and positive electrodes during formation and after cycling have been thoroughly analysed by X-ray photoelectron spectroscopy (XPS) and correlations to the electrochemical differences observed between electrolytes has been proposed.

2. Experimental

The materials and methods used in this study are fully described in the supplementary information section and identical to those described in Madec e*t al*.[24] For the Gas chromatography coupled with electron impact mass spectroscopy (GC-MS) study, fully described procedures can also be found in reference 24 and 43.

For the computational study, the geometries of isolated solvent (EC and EMC) and electrolyte additive (VC and ES) molecules and their clusters including a lithium ion were optimized at the level of B3LYP/6-311+G(2d,p) in the gas phase. A total solvation number of four was assumed to build the clusters.

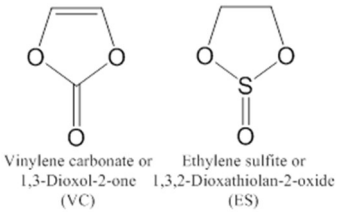

Figure 1. Molecular formula and structural information for VC and ES.

The solvation energies (in kcal mol^{-1}) were calculated at the MP2/6-311+G(2d,p) level as follows:

$$\Delta E_{solv} = E_{elec}\,[Li^+(S)_4] - E_{elec}\,[Li^+] - 4\,E_{elec}\,[S] \quad (1)$$

where E_{elec} [$Li^+(S)_4$], E_{elec} [Li^+] and E_{elec} [S] represent the electronic energies for $Li^+(S)_4$, Li^+ and S (S = EC, EMC, VC or ES), respectively.

The solvent reduction energies (in kcal mol^{-1}) without or with Li were calculated at the MP2/6-311+G(2d,p) level as follows:

$$\Delta E_{red} = E_{elec}[S^-] - E_{elec}[S] \quad (2)$$

$$\Delta E_{red}^{Li} = E_{elec}[LiS] - E_{elec}[Li^+S] \quad (3)$$

where E_{elec} [S] and E_{elec} [Li^+ S] are the electronic energies for S and Li^+S before reduction, and E_{elec} [S^-] and E_{elec} [LiS] are the corresponding electronic energies after reduction, respectively.

For the schematic representations of the SEI films, the SEI thicknesses were estimated using the relative intensity of the active material features, *i.e.* the lithiated graphite C 1s and the NMC O 1s features at ~ 282.6 eV and 529.5 eV, respectively. The relative intensity was defined as:

$$I_{rel} = \text{at. \% (sample)} / \text{at. \% (fresh)} \quad (4)$$

Where at. % (sample) and at. % (fresh) are the atomic percentages for the active material feature of a given sample and for the fresh electrode, respectively, as determined from XPS quantification. Assuming a simple model where the SEI layer was considered as homogenous in thickness (d) with no porosity and with an average composition, the SEI thickness was then estimated as:

$$I_{rel} = e^{-d/\lambda} \quad (5)$$

where the inelastic mean free path (IMFP), λ, was estimated by averaging values for polyacetylene, LiF and polyethylene.[44,45] This procedure yields λ = 2.7 nm and 2.1 nm for photoelectron kinetic energies of ~ 1000 eV (C 1s) and ~ 700 eV (O 1s) used in this study.

3. Results and discussion

3.1 Reactivity of the additives

In this section, the reactivity of ES and VC alone or in combination during the early stage of the formation cycle was investigated by combining d*Q*/d*V vs. V* and GC-MS analysis as well as theoretical calculations.

Figure 2a shows the differential capacity (d*Q*/d*V*) *vs. V* curves of NMC/graphite pouch cells between 1.6 and 3.5 V of the formation cycle for control, VC and ES-containing electrolytes. These plots allow a better determination at which cell terminal voltage the additives initially react with the partially lithiated graphite. Control cells showed a pronounced peak at 2.75 V (graphite at ~ 0.8 V vs. Li/Li^+) attributed to the reduction of EC at the surface of the graphite electrode.[46,47]

When 2% VC was added, this peak was almost suppressed suggesting that VC nearly eliminates the electrochemical degradation of EC. A peak appeared, however, at a lower cell voltage of ~ 2.65 V (graphite at ~ 0.9 V vs. Li/Li^+) and is assigned to the reduction of VC.[22,24] This result is in agreement with the beginning of the consumption of VC at 2.4 V (~ 9%) and its further consumption at 3.5 V (~ 55%) as measured by GC-MS (Figure 3a).[24,48] Moreover, the use of VC totally suppressed the transesterification of EMC into DEC and DMC as measured by GC-MS (Figure 3c) compared to control electrolyte for which about 40% of EMC was converted at 3.5 V.[24,48] Note that this phenomenon has been widely reported and described in Li-ion cells.[49,50,51,43,52] The use of VC also nearly suppressed (< 0.1%) the addition products of EC with EMC, DEC and DMC observed from GC-MS analysis that accounted for 1-3% of the total electrolyte weight for control electrolyte.[24,48,53]

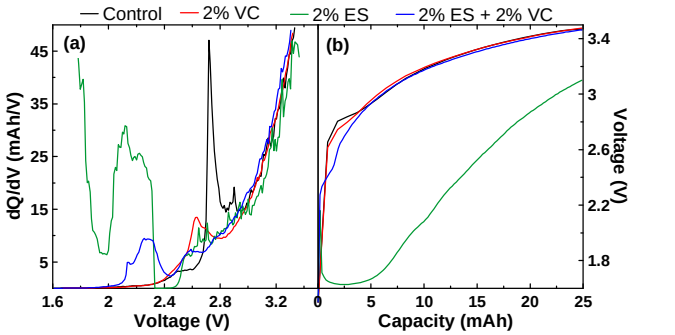

Figure 2. (a) Differential capacity (d*Q*/d*V*) versus voltage (V) during the early stages of the formation cycle of the 240 mAh NMC/graphite pouch cells at C/20 and 40°C for the different electrolytes; (b) cell voltage versus capacity during the first 25 mAh of the formation cycle.

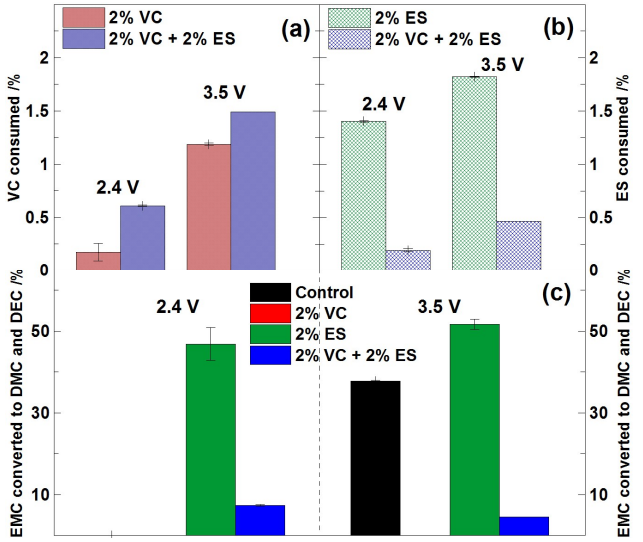

Figure 3. Amount of (a) VC and (b) ES consumed in NMC/graphite pouch cells after formation at 2.4 V and 3.5 V. (c) Amount of EMC converted into DMC and DEC in NMC/graphite pouch cells for the different electrolytes after formation at 2.4 V and 3.8 V.

For cells with 2% ES (Figure 2a), a massive feature was observed near 1.8 V (graphite at ~ 1.7 V vs. Li/Li^+) which corresponds to a sharp decrease in the voltage versus capacity curve (Figure 2b) and is assigned to a vigorous reduction of ES.[40] This is supported by the large consumption of ~ 65% of ES after formation at 2.4 V (Figure 3a). The reduction of ES might be initiated from 1.5 V as during the 24 h hold step at 1.5 V of the formation process, cells with 2% ES electrolyte showed a capacity of about 2 mAh compared to about 1 mAh for control and VC-containing electrolytes (See Table S1). Additionally, the initiation of the ES reduction may involve the copper current collector as at 2.4 V, cells with 2% ES showed two doublets on the Cu 2p XPS core spectrum of the graphite electrode (see Figure S4). Note that no Cu was observed after formation

above 2.4 V and when VC was added to ES, no Cu was found. After formation at 3.5 V, cells with 2% ES showed almost a total consumption of the ES molecules (~ 85%). Moreover, for ES alone, the conversion of about 47% of EMC into DEC and DMC was observed at only 2.4 V compared to ~ 40% at 3.5 V for control electrolyte. The addition products of EC with EMC, DEC and DMC were also found in the same range as for control cells (1-3 wt%) but occured at only 2.4 V. As a whole, these results clearly indicate a higher and different reactivity of the electrolyte components when ES was used alone.

When VC was added to ES (Figure 2a), the massive feature at 1.8 V was totally suppressed and three peaks were instead observed at 2.15 V, 2.3 V and 2.6 V (graphite at ~ 1.45 V, 1.3 V and 1.0 V vs. Li/Li^+, respectively). Although it is difficult to assign these peaks to a specific reaction of VC or ES, it is clear that the addition of VC to ES almost suppressed the reactivity of ES in agreement with the consumption of only ~ 9% of ES at 2.4 V compared to ~ 65% when ES was used alone (Figure 3b). By combining ES to VC, the reactivity of VC was also modified as a higher consumption of ~ 30% of VC was observed at 2.4 V compared to ~ 9% for VC alone (Figure 3a). At 3.5 V, these two phenomena were still observed and the total consumption of ES remained relatively low (less than 25%, Figures 3a and b). The conversion of EMC into DEC and DMC was observed at both 2.4 and 3.5 V more likely due to the reactivity of ES with however, a lower extend (5 - 8 %) compared to ES alone (about 47%) due to the beneficial effect of VC. The addition products of EC with EMC, DEC and DMC were also significantly decreased when VC was added to ES (< 1%) but not as much as for VC alone (< 0.1%).

The d*Q*/d*V vs. V* and GC-MS results therefore suggest a very strong impact of these two additives on their reactivity when used in combination with a dominant role of VC. To get insight on the reactivity of VC and ES, the reduction energy (kcal mol^{-1}) and the lithium solvation energy (kcal mol^{-1}) were then calculated for the different electrolyte solvents (EC, EMC) and additives (ES, VC) (Table 1). Table 1 shows that ES had the lowest reduction energy both with and without lithium. ES is therefore most preferentially reduced among the electrolyte solvents and additives used in this study which explain the vigorous reaction observed on the *dQ/dV* vs. *V* curves (Figure 2a) when ES was used alone. This result is in agreement with a recent study by Bhatt *et al*.[38] showing that in PC electrolyte, ES is preferentially reduced compared to VC from the lowest unoccupied molecular orbital (LUMO) energies and from both the first and second electron reduction energies. They postulate that it is probably due to the stability of the $–SO_3$ group in the case of ES compared to the $-CO_3$ group for EC. Table 1 also shows that VC was more likely reduced in the presence of Li^+ than ES without Li^+. Additionally, the Li^+ solvation energy was in the order EC > VC > ES > EMC (Table 1) which indicates a preferential solvation of Li^+ by VC compared to ES when both additives are used in combination. Therefore, when VC is added to ES, VC becomes therefore more likely reduced compared to ES which explains the suppression of the vigorous reaction of ES observed when VC was added (Figures 2a and 3b) and the higher consumption of VC measured by GC-MS (Figure 3a).

Table 1. Reduction energy (ΔE_{red}, kcal.mol^{-1}) without and with Li for the different electrolytes components (EC, VC, ES, EMC) calculated in the gas phase at the MP2/6-311+G(2d,p) level. Li solvation energy (ΔE_{solv}, kcal.mol^{-1}) for $Li^+(S)_{n=4}$ (S = EC, VC, ES, EMS) calculated in the gas phase at the MP2/6-311+G(2d,p) level. The geometry was optimized at the B3LYP/6-311+G(2d,p) level. *solvent + e^- → solvent$^-$. **Li^+-Solvent + e^- → Li-solvent.

	EC	VC	ES	EMC
ΔE_{red}, without Li* (kcal.mol^{-1})	26.9	26.4	-0.7	34.9
ΔE_{red}, with Li** (kcal.mol^{-1})	-89.5	-88.1	-131.8	-91.5
ΔE_{solv} (kcal.mol^{-1})	-47.1	-43.9	-42.7	-42.6

3.2 Gas analysis

In this section, the gas volume generated during both formation and cycling as well as the nature of the gaseous species produced during the formation cycle were studied to compare and understand the impact of the different electrolytes on the gas production.

Figures 4a and b show the gas volume versus cell voltage (V) and the gas volume versus capacity during the first 25 mAh of the formation cycle, respectively. Figure 4a shows that during formation, cells with control electrolyte produced about 0.9 mL of gas. Cells with 2% ES produced a significantly larger amount of gas (more than 3 mL) which is critical for a pouch cell that has an initial volume of 2.2 mL and is assigned to the vigorous reaction of ES (Figure 2a). Cells with VC alone or in combination with ES produced, however, very low amount of gas (about 0.25 mL) which means than VC acts as a gas reducing agent more likely due to the suppression of the EC reduction during formation (Figure 2a). Note that during formation, all cells showed a small decrease of the volume of gas above 3.6-3.8 V (Figure 4a) probably be due to the reaction of gas during the formation of the SEI film at the graphite surface as suggested recently by Self *et al*.[54]

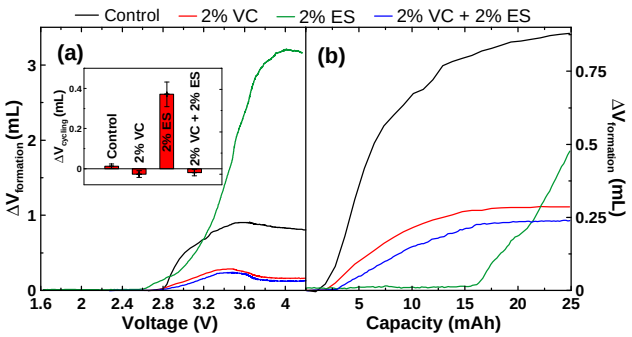

Figure 4. (a) Gas volume versus cell voltage (V) during the first charge of the formation cycle for NMC/graphite pouch cells containing different electrolytes; (b) gas volume versus capacity during the first 25 mAh of the formation cycle. Inset of figure 4a: Volume of gas evolved during the UHPC cycling at 11 mA (C/20) and 40.0 ± 0.1 °C for the NMC/graphite pouch cells containing the different electrolytes. A positive value means the cells are swelling while a small negative value indicates that the cell volume slightly shrinks.

The inset of Figure 4a shows that during the UHPC cycling, both control and VC cells showed very small volume changes

while cells with ES continued to produce a large volume of gas (about 0.4 mL) which indicates the formation of non-passivating SEI film at the graphite and/or the NMC surfaces. Also, when VC was combined to ES, the production of gas during cycling was similar to VC alone indicating again the dominant role of VC on the SEI films formation.

Figure 4a also shows that the onset voltage of the gas production for cells with 2% ES was 2.6 V which means that the vigorous reduction of ES near 1.8 V (Figures 2a and b) does not produce gas. Additionally, the capacity associated with the reduction of ES before the production of gas (i.e. below 2.6 V) was ~ 16.2 mAh (Figure 4b). This capacity would correspond to a 4-electron reduction mechanism of ES assuming that each molecule of ES in the cell reacts.[40] Recall that only ~ 65% and ~ 85% of the ES molecules in the cell had reacted at 2.4 V and 3.5 V, respectively (Figure 3b). Therefore, it is more likely that ES molecules react through different reduction mechanisms not necessarily involving 4-electrons. This assumption is supported by the S 2p core spectra analysis as will be discussed later. This result therefore disagrees with the theoretical calculations of Xing *et al*.[36] and Leggesse *et al*.37 who predicted a 1-electron and a 1 or 2-electrons reduction mechanism of ES in PC-containing electrolytes, respectively. When VC was added to ES, the onset voltage of the gas production was 2.8 V and matches those of control and VC cells (Figure 4a). Moreover, the capacity before the gas production was only ~ 2.5 mAh (Figure 4b). Therefore, when VC is added to ES, the preferential reduction of VC allows to hinder the vigorous reaction of ES and the resulting gas production.

Figure 5 shows the GC-MS peak areas for the primary gaseous species extracted at room temperature from the NMC/graphite pouch cells after formation at 2.4 V and 3.5 V. The complete data set is also included in Figure S5 for information. Although no apparent formation of gas was expected before 2.6 V from the *in-situ* gas measurements (Figure 4a), the extraction procedure using low pressure forces any gases out of the pouch cell to be analyzed. A fully described reaction scheme of the reactions mentioned in the present study can be found in reference 43.

At 2.4 V (Figure 5a), all electrolytes showed CO_2 as the most abundant gas with small amounts of ethene and CO (Figure S5). Also, both control and VC electrolytes showed no additional gases at 2.4 V due to their low reactivity below 2.4 V (Figure 2a). At 3.5 V (Figure 5b), the nature of the gases was significantly different while the production of gas was measurable (Figure 4). Ethene became the most abundant gas except for ES alone for which the amount of CO_2 was similar. Small amounts of ethane and CH_4 (Figure S5) were also observed at 3.5 V for all electrolytes. While the formation of ethene is assigned to the reduction of EC at the graphite surface[46,55,56], ethane is, however, preferentially formed via the reduction of the linear carbonate EMC.[55,56] The source of hydrogen involved in the formation of ethane and other compounds was recently attributed to dialkyl carbonates that were found to be prone to H radical abstraction in the presence of alkyl radicals.[57] For control electrolyte, the amount of ethane was about two orders of magnitude lower than ethene which indicates that EC is more easily reduced at the graphite surface than EMC as expected from Table 1.[56] At 3.5 V, control cells also showed small amounts of additional gases such as methyl formate and ethyl formate for instance (Figure 5 and S5) that are attributed to the reduction of EMC.[43]

When 2% VC was used, the production of ethene was lowered at both 2.4 V and 3.5 V compared to control electrolyte due to the preferential reduction of VC at the graphite surface that supressed the EC reduction as expected (Table 1 and Figure 2a).[20] The formation of CO_2 was, however, increased by the addition of VC due to its specific reactivity.[20] At 3.5 V, the addition of VC also decrease the amount of ethane and supressed the formation of the additional gases observed for control electrolyte. VC therefore forms a passivating SEI film at the graphite surface that hinders the parasitic reactions from the solvents.

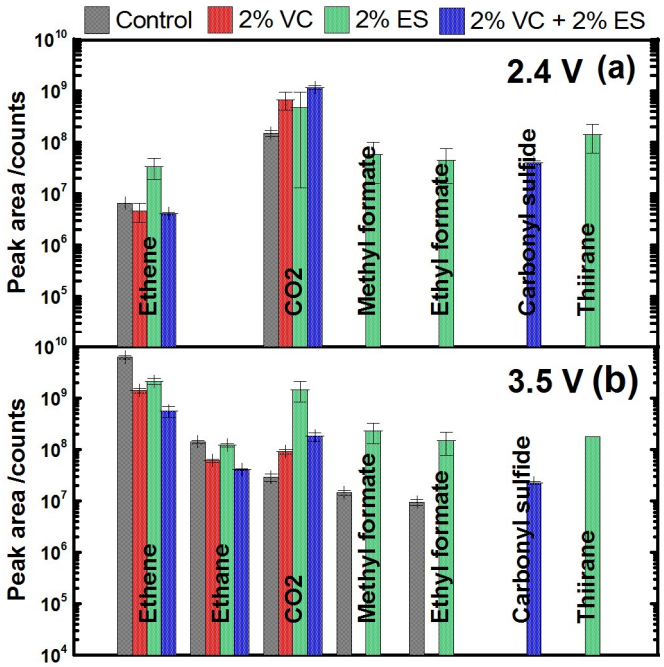

Figure 5. GC-MS data for the primary gases extracted from NMC/graphite pouch cells for the different electrolytes after formation at (a) 2.4 V and (b) 3.5 V. The data presented here shows the normalized peak area for compounds that are gaseous at room temperature.

For cells with 2% ES, all gases detected for control electrolyte were observed with a significantly higher amount except for ethane and ethane at 3.5 V. Also, some of these gases such methyl formate and ethyl formate were detected as soon as 2.4 V compared to 3.5 V for control electrolyte (Figure 5 and S5) which could be attributed to a higher reactivity of EMC at a lower voltage when ES is used, in agreement with the transesterification of EMC observed by GC-MS (Figure 3c). Note that if each ES molecule eventually leads to one molecule of gas that obeys the ideal gas law, the volume of gas produced would be 3.5 mL. However this larger production of

gas with ES alone cannot be explained only by the reaction of the ES molecules. Indeed, Figure 4a showed that the vigorous reaction of ES near 1.8 V (Figure 2a) did not generate gas before 2.6 V which implies that the production of gas may be initiated by another reaction such as the expected reduction of EC around 2.6 V. It is therefore suggested that the larger production of gases is due to both the vigorous reaction of ES and a larger reactivity of EC at the surface of the graphite electrode. Figure 5 also shows that cells with 2% ES produced a cyclic sulfur-containing compound, thiirane or ethylene sulfide (C_2H_4S), that was the second most abundant gas at 2.4 V indicating a strong reactivity of the additive ES. Cells with ES alone also generated small amounts of additional gases that were not observed with other electrolytes such as methanol, ethylene oxide, dimethoxymethane, etc. (Figure S5). The formation of these gases could be assigned to the reduction of EC or EMC[58] as well as ES which again highlights the higher reactivity of both EC and EMC when ES is used.

When VC was added to ES, a completely different gas formation pathway was observed. First, the production of ethene was further decreased while the amount of CO_2 was further increased compared to control and VC electrolytes due to the higher consumption of VC when combined with ES (Figure 3a). Secondly, the addition of VC to ES totally suppresses the formation of the additional gaseous compounds that were observed for ES alone. For instance, no thiirane was found but a new sulfur compound, carbonyl sulfide (O=C=S) was observed as soon as 2.4 V. These results therefore indicate that when VC is added to ES, VC dominates the SEI film formation process and hinders the reactivity of ES.

3.3 Electrochemical performance

Figure 6 shows a summary of the coulombic inefficiency (1 – CE), charge end point capacity slippage rate (in mAh/cycle) and voltage drop during storage of the NMC/graphite pouch cells. The short-term CIE and charge slippage were used here to rank cells by their projected lifetime.[17,59] Figure 7 shows that the addition of 2% VC greatly improved all the performance compared to control electrolyte.[14,17] When 2% ES was used, however, worse performance than control cells was observed. For instance, cells with 2% ES showed a very poor coulombic efficiency (less than 0.977) compared to about 0.995 for control electrolyte. Cells with 2% ES also showed a 5 to 10 times higher charge endpoint capacity slippage during cycling as well as a 2 to 4 times higher voltage drop during storage compared to control and VC electrolytes. These results, in addition to the large production of gas during cycling (Figure 4a) clearly indicate the formation of a non-passivating SEI film at the NMC surface when ES is used alone as discussed in the XPS section. When VC was added to ES, similar performance was observed compared to VC alone which confirms the dominant role of VC on the SEI film formation process at both electrodes. Similar SEI films can therefore be expected at the surface of both graphite and NMC electrodes in VC and VC + ES electrolytes.

Figure 7 shows the discharge capacity for the short term cycling at 40°C and C/20 for NMC/graphite pouch cells with the different electrolytes. Although the discharge capacity over the short term was well-maintained for all cells except those with 2% ES (Figure 7a), some trends can be observed in good agreement with the UHPC data (Figure 6). Cells with control electrolyte showed the highest discharge capacity fade while the addition of 2% VC greatly improved the discharge capacity retention. Cells with 2% ES showed an odd behavior with an increase of capacity between cycles 4 and 10 followed by a slight capacity fade. However, cells with ES showed anomalously low capacity during the entire short term cycling which can be partially explained by a loss of pressure on the electrode stack due to the large production of gas during cycling (Figure 4a). When VC was added to ES, although a higher capacity retention was not expected from the UHPC data (Figure 6) compared to VC alone, it can be attributed to the lower impedance observed by Xia *et al.*[40] when VC was combined to ES.

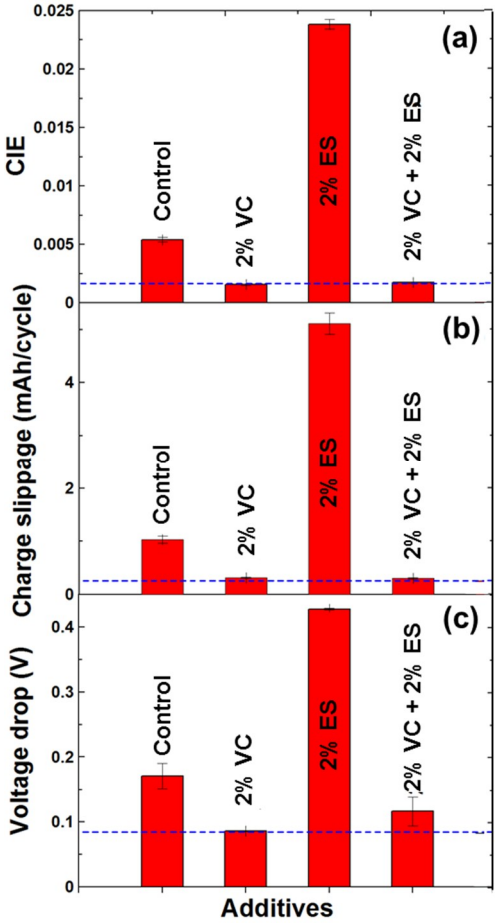

Figure 6. Summary of the high precision cycling and storage data for the NMC/graphite pouch cells studied here: (a) coulombic inefficiency (CIE) and (b) charge end point capacity slippage during cycling between 2.8 and 4.2 V at C/20 and 40. ± 0.1°C as well as (c) voltage drop during 500 h of storage at 4.2 V and 40. ± 0.1°C.

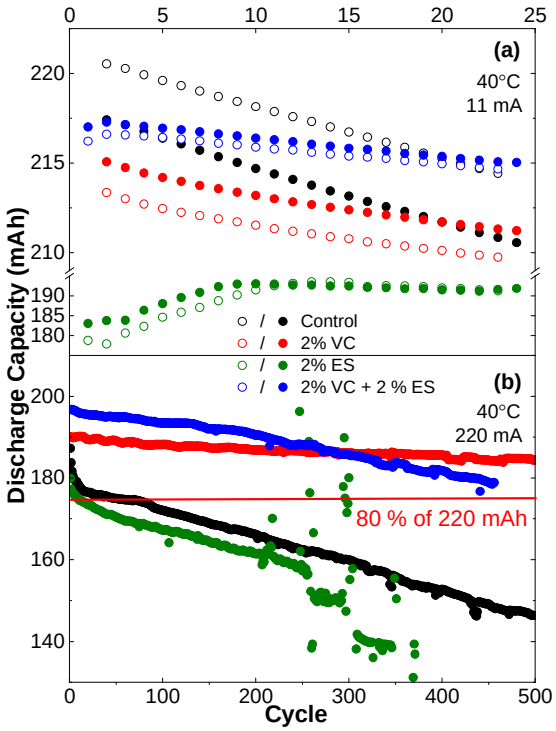

Figure 7. Discharge capacity versus cycle number for NMC/graphite pouch cells (220 mAh) with different electrolyte additives as indicated when cycled between 2.8 and 4.2 V at 40.0 ± 0.1°C and (a) 11 mA (C/20) and (b) 220 mA (C).

Figure 7b shows the discharge capacity for the long term cycling at 40°C and C for NMC/graphite pouch cells with the different electrolytes. 2% VC greatly improved the discharge capacity retention compared to control electrolyte for which the initial capacity falls below 80% after only 75 cycles. Although cells with 2% VC + 2% ES showed similar capacity retention as the 2% VC cells up to 200 cycles, beyond 200 cycles, a decrease of the capacity retention was observed for cells with VC + ES. Cells with 2% VC therefore showed the best capacity retention with more than 180 mAh after 500 cycles. Contrary to the short term cycling, the addition of 2% ES to 2% VC had no beneficial effect. It is believed that the amount of ES (2%) is too large for long term cycling as Xia *et al*.[40] reported very close capacity retention after 500 cycles at 40°C and C for cells with 2% VC and 2% VC + 1% ES. Based on these electrochemical and gas results and the previous work by Xia *et al*.[40], it is concluded that either 2% VC or 2% VC + 1% ES may have a beneficial impact for practical application.

3.4 XPS analysis

The role of ES used either alone or in addition with VC on the electrode/electrolyte interfaces was investigated by XPS in order to understand how those interfaces are correlated to the electrochemical performance. For control (*i.e*. without additive) and VC electrolytes, the results described hereafter follow our previous study on NMC/graphite pouch cells.[24] For the different electrolytes, the SEI films were analyzed both during formation at 2.4 V, 3.8 V, 4.2 V during charge and 2.8 V during discharge as well as after 25 cycles at both 4.2 V during charge and 2.8 V during discharge (referred to as C4.2 V and D2.8 V, respectively).

3.4.1 Graphite negative electrodes. Figure 8 shows the C 1s and O 1s core spectra of the graphite electrodes from cells with 2% ES or 2% VC + 2% ES electrolytes compared to control and 2% VC electrolytes during formation and after 24 cycles. Enlarged C 1s and O 1s core spectra of graphite electrodes during formation at 2.4 V and 3.8 V are shown in Figures S6 and S7 so that readers can take a closer look at the data. The C 1s core spectrum of the fresh electrode (*i.e.* without electrolyte) showed five components at 284.1, 285, 286.9, 288.6 and 290.8 eV attributed to the C=C bonds from the graphite, the C-C/C-H from the SBR binder, the C=O and COOR carbons as well as the ''shake up'' satellite from the graphite, respectively[60,61] The O 1s core spectrum of the fresh electrode showed two peaks at 531.6 and 533.4 eV assigned to the two oxygen atoms of the CMC binder.[22] At 2.4 V, all electrolytes showed very close C 1s spectra compared to the fresh electrode which indicates that almost no SEI is formed on the graphite surface at this voltage. On the O 1s core spectra, however, a clear evolution between the different electrolytes was observed. For control and 2% VC electrolytes, no significant difference was observed compared to the fresh electrode while for cells with 2% ES, the two O 1s peaks from the fresh electrode were replaced by two new peaks at 532 and 533.7 eV. The origin of these peaks is discussed latter. The use of 2% ES therefore forms a thin (as inferred by the C 1s spectra) SEI film at the graphite surface at a lower voltage than control and 2% VC cells, in agreement with the vigorous reaction of ES below 2.4 V (Figure 2). When 2% VC was added to 2% ES, an intermediate evolution of the O 1s components was observed. The new component at 532 eV was visible with, however, a lower intensity compared to 2% ES alone while the second main component remained at 533.4 eV as for the fresh electrode. These results already indicate the dominant role of VC when combined with ES. Moreover, at 2.4 V, 2% VC + 2% ES electrolyte showed a third O 1s peak at very high binding energy (534.5 eV) attributed to the formation of an oligomer of VC (called Oligo-VC thereafter) at the surface of the graphite surface.[20,22,24] Note that the expected C 1s peaks of such Oligo-VC were, however, not visible at 2.4 V probably due to their very weak contribution. For 2% VC electrolyte, no Oligo-VC component was observed at 2.4 V probably due to the 3 times lower consumption of VC at this voltage compared to 2% VC + 2% ES electrolyte (Figure 3a).

During the rest of the first charge (at 3.8 V and 4.2 V), a significant decrease of the intensity of the graphite peak was observed for each electrode blend indicating the further formation of a SEI film at the graphite surface. At 4.2 V, based on the graphite peak relative intensity, it appears that the SEI thickness is higher for control electrolyte and lower for ES-containing electrolyte while 2% VC gives the thinner SEI film. After discharge to 2.8 V, the intensity of the graphite peak was partially recovered for control electrolyte (*i.e*. the SEI thickness decrease) due to the dissolution/consumption of SEI species while 2% VC stabilized the SEI film (from a thickness perspective anyway). For ES-containing electrolytes, however,

the intensity of the graphite peak increased after discharge indicating a relatively less stable SEI compared to VC alone, probably due to the ES reactivity. After cycling, no graphite was observed for control and 2% ES electrolytes while for VC-containing electrolytes, the graphite peak was slightly visible indicating a more passivating SEI film when VC was used.

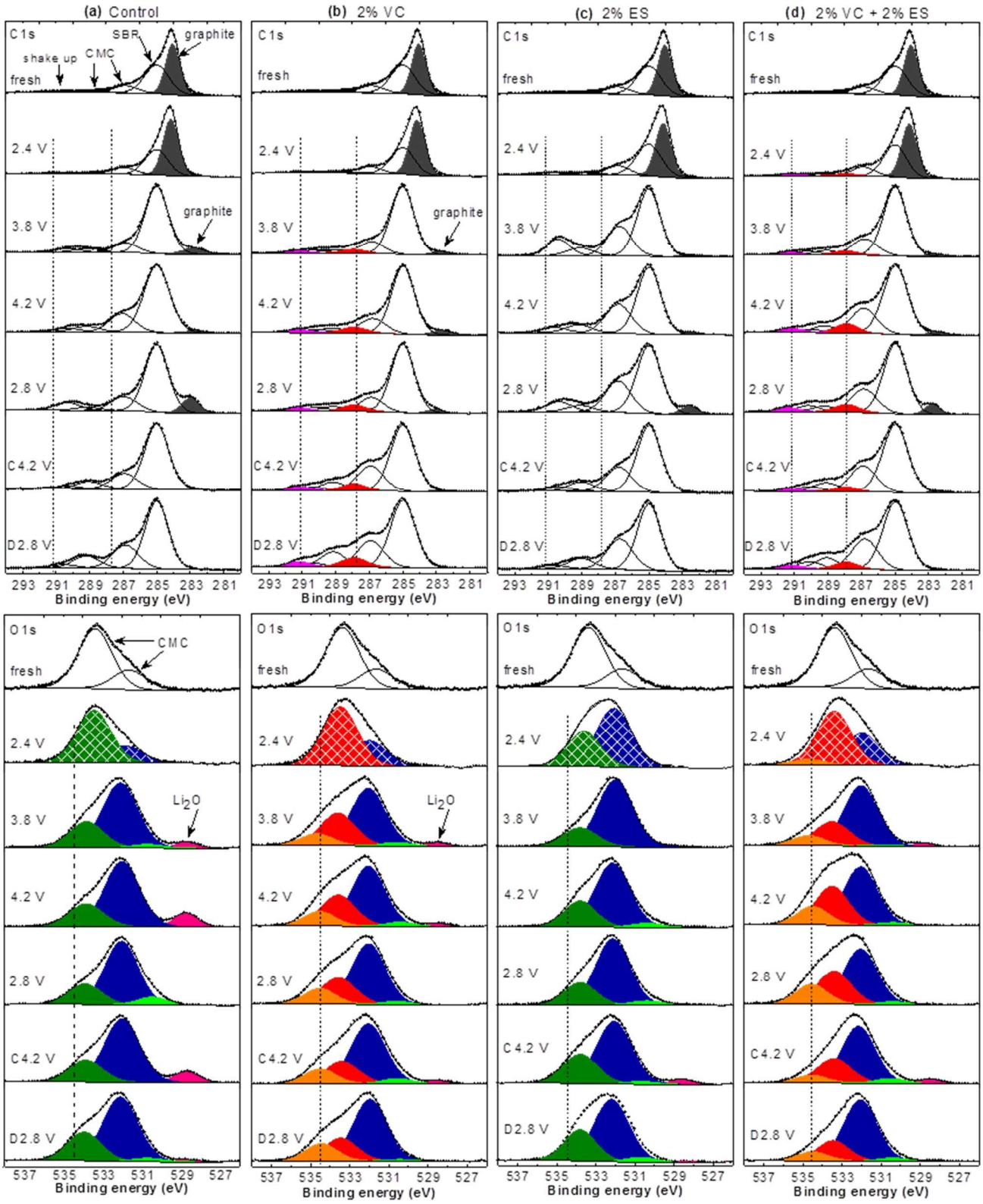

Figure 8. C 1s and O 1s XPS core spectra for graphite electrodes with (a) control, (b) 2% VC, (c) 2% ES, and (d) 2% VC + 2% ES electrolytes taken from cells during formation at 2.4 V, 3.8 V and 4.2 V during charge and 2.8 V during discharge as well as after cycling at 4.2 V during charge (C4.2 V) and at 2.8 V during discharge (D2.8 V) at C/20 and 40. ± 0.1°C. In the C 1s core spectrum of the fresh electrode, the five components at 284.1, 285, 286.9, 288.6 and 290.8 eV are attributed to the C=C

bonds from the graphite, the C-C/C-H species from the SBR binder, the C=O and COOR carbons as well as the ''shake up'' satellite from the graphite. In the O 1s core spectrum of the fresh electrode, the two peaks at 531.6 and 533.4 eV are assigned to the two oxygen atoms of the CMC binder.

In the 286 - 292 eV range of the C 1s spectra of the graphite electrodes (Figure 8), all electrolytes showed the appearance at 286.9, 289.2 and 290.3 eV of CO^-, CO_2^- and CO_3-like carbon environments in agreement with the formation of carbonaceous species (*i.e.* degradation products of EC and/or EMC) at the graphite surface. However, no clear evolution in peak intensity with the state of charge can be observed. Importantly, both 2% VC and 2% VC + 2% ES electrolytes showed two additional C 1s components at 287.9 and 291.3 eV with a 2:1 ratio that are attributed to the formation of an Oligo-VC at the graphite surface.[22,24]

After formation at 3.8 V, for all electrolytes, the two O 1s peaks of the fresh electrode at 531.6 and 533.4 eV were replaced by two new main components at 532 and 533.8 eV. This can be explained by the covering of the CMC binder at the same time as the graphite while the SEI is formed.[22] The peak at 532 eV is attributed to CO_2-like oxygen from carbonate compounds such as lithium ethylene dicarbonate $(CH_2OCO_2Li)_2$ (LEDC)[62,63] formed by reduction of EC and/or other lithium alkyl carbonates ($ROCO_2Li$) including lithium carbonate formed by the reduction of EC and/or EMC. The second peak at 533.5 - 533.8 eV is assigned to -C-O- bonds from $ROCO_2Li$ and/or ether derivatives.[64,65] More details about the corresponding multistep degradation mechanisms of carbonate-based electrolytes can be found in the literature.[50,43,66,67] In the case of VC-containing electrolytes (Figure 8b and d), the second peak at 533.8 eV was slightly shifted to 533.5 eV due to a specific reactivity of VC at the graphite surface.[22] For all electrolytes, two additional peaks were observed at 530.7 and 528.6 eV and assigned to the formation of lithium alkoxide (ROLi) and lithium oxide (Li_2O), respectively.[68,69] Although the exact formation pathway of Li_2O is rather difficult to clarify, according to our previous work, the formation of Li_2O from water through $H_2O + 2Li^+ + 2e^- \rightarrow Li_2O\ (s) + H_2\ (g)$, is unlikely here.[24] Instead, Li_2O is more likely forms from further reduction of carbonate degradation compounds[64,70] as Li_2O was formed during charge both during formation and after cycling while the SEI thickness increased (see graphite peak evolution during formation). When either VC or ES was used, the reaction pathway that leads to Li_2O is almost suppressed indicating a positive impact of both VC and ES on the suppression of some parasitic reactions at the electrolyte/graphite interface. After formation at 3.8 V, VC-containing electrolytes also showed an additional component at 534.5 eV attributed to the formation of Oligo-VC.

3.4.2 Positive $LiNi_{1/3}Mn_{1/3}Co_{1/3}O_2$ electrodes. The C 1s XPS core spectra of NMC electrodes are dominated by PVdF and carbon black contributions which leads to difficult interpretation.[24,71] For this reason and based on our previous work[24], Figure 9a shows only the overlay of the C 1s core spectrum of the fresh NMC electrode (black) as well as the typical C 1s core spectra for electrodes from cells with 2% ES (blue) and 2% VC + 2% ES (green) electrolytes taken after 24 cycles at 2.8 V during discharge. Figure 9a (bottom) also shows the difference spectrum between 2% VC + 2% ES and 2% ES for thorough comparison. The C 1s core spectrum of the fresh electrode showed five components. The peaks at 284.5, 287.4 and 288.6 eV are attributed to the C=C, C=O and COOR bonds from the carbon black, respectively.[60,61] The peaks at 286.0 and 290.5 eV are assigned to the CH_2 and CF_2 bonds from the PVdF binder, respectively. Cells with 2% ES showed a small increase of intensity in the 285 - 290.5 eV range compared to the fresh electrode due to the formation of an SEI film at the NMC surface. For 2% VC + 2% ES electrolyte, however, a significantly higher intensity was found indicating a relatively thicker SEI. This was highlighted by the difference spectrum (bottom of Figure 9a) that clearly shows a much higher contribution of SEI components at 285.3 (C-C/C-H), 286.9 (CO-) and 289 eV (CO_2-) from carbonaceous species. This result is confirmed by the 76 - 44 eV XPS spectra (Figure 9b) that shows a 3.5 times lower intensity of the Ni, Co and Mn 3p peaks from the NMC material when 2% VC + 2% ES was used compared to 2% ES alone. The difference spectrum also revealed two additional components at 287.9 and 290.9 eV with a 2:1 ratio for 2% VC + 2% ES electrolyte, in good agreement with the formation of Oligo-VC at the NMC surface.[22] Note that this feature was also observed for other states of charge during formation and after.

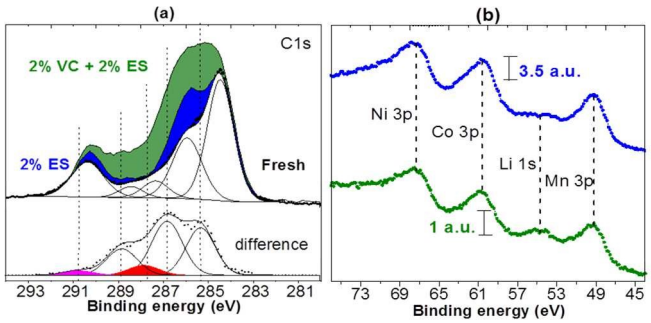

Figure 9. (a) Typical C 1s XPS core spectra of $LiNi_{1/3}Mn_{1/3}Co_{1/3}O_2$ electrodes for the fresh electrode (black) as well as from cells with 2% ES (blue) and 2% VC + 2% ES (green) electrolytes taken after 24 cycles at 2.8 V during discharge. The bottom shows the corresponding difference spectrum between 2% VC + 2% ES and 2% ES electrolytes. (b) Core XPS spectra in the 76 - 44 eV range (showing the Ni 3p, Co 3p, Mn 3p and Li 1s components) for NMC electrodes taken from cells with 2% ES (blue) and 2% VC + 2% ES (green) after 24 cycles at 2.8 V during discharge.

Figure 10 shows the O 1s core spectra of the NMC electrodes from cells with 2% ES or 2% VC + 2% ES electrolytes compared to control and 2% VC electrolytes during formation and after 24 cycles. Enlarged O 1s core spectra of NMC electrodes during formation at 2.4 V and 3.8 V are shown in Figure S8 so that readers can take a closer look at the data. The O 1s spectrum of the fresh electrode showed two components. The peak at 529.5 eV is attributed to O^{2-} anions from the lattice oxygen of

the NMC material while the peak at 531.5 is assigned to oxygen anions with deficient coordination at the NMC surface (''surface oxygens'')[22] and/or CO_x-like oxygen from the carbon black[60,61]. At 2.4 V, both control and 2% VC electrolytes showed no significant difference compared to the fresh electrode indicating that almost no SEI is formed on the NMC surface. For ES-containing electrolytes, however, the O 1s peaks from the fresh electrode at 531.5 eV was replaced by two new peaks at 531.7 and 533.5 eV indicating that the use of ES initiates the formation of an SEI film at the NMC surface as soon as 2.4 V. After formation to 4.2 V, all electrodes showed a decrease of the O 1s peak from the NMC at 529.5 eV attributed to the continuous formation of an SEI film at the NMC surface. Based on the NMC peak intensity, the SEI thickness at 4.2 V follows 2% VC+ 2% ES > 2% VC > control > 2% ES. After cycling, the intensity of the NMC peak is higher for 2% VC compared to control electrolyte which suggests that the VC stabilized the SEI film and hinder parasitic reactions at the NMC surface which explain the better electrochemical performance (Figures 7 and 8). These results can also explain the decrease of the impedance at the NMC/electrolyte interface when VC was used as observed recently by symmetric cells study.[16,72,73] When ES was added to VC (Figure 10d), based on the NMC peak intensity, a slightly less stable SEI was formed as the SEI thickness continued to increase after cycling. For ES alone (Figure 10c), however, the intensity of the NMC peak remained close and constant compared to the fresh electrode during both formation and cycling. This result therefore highlights a special reactivity of the 2% ES electrolyte towards the NMC electrode. Despite an apparent thin and stable SEI film on the NMC surface with ES alone, the SEI does not prevent parasitic reactions to occur at the electrolyte/NMC interface considering the electrochemical performance (Figure 6) which also explain the large production of gas (Figure 4).

Considering the two new O 1s components at 531.7 and 533.5 eV, they were observed for all electrolytes at 3.8 V. In the case of VC-containing electrolytes, the peak at 533.5 eV was shifted to 533.1 eV due to a specific reactivity of VC.[22] The peak at 531.7 is attributed to CO_2-like oxygen from carbonate compounds ($ROCO_2Li$) in addition to any remaining contribution of the ''surface oxygens'' from the NMC material[22] and/or CO_x-like oxygen from the carbon black[60,61]. The peak at 533.5 - 533.1 eV is assigned to C-O bonds from ether derivatives[64,65] and/or $ROCO_2Li$. The peak at 531.7 eV showed no apparent evolution while the intensity of the 533.5 - 533.1 eV peak greatly increased during charge between 3.8 and 4.2 V and decreased after discharge except for 2% ES. After cycling, however, no significant change was observed between charge and discharge. These results suggest the formation of less stable SEI compounds at 533.5 - 533.1 eV. After cycling, the amount of these species was higher for control than for VC-containing electrolytes which emphasizes the passivating role of VC. VC-containing electrolyte also showed an additional peak at a very high binding energy of 534.2 eV due to the formation of Oligo-VC.[22,24]

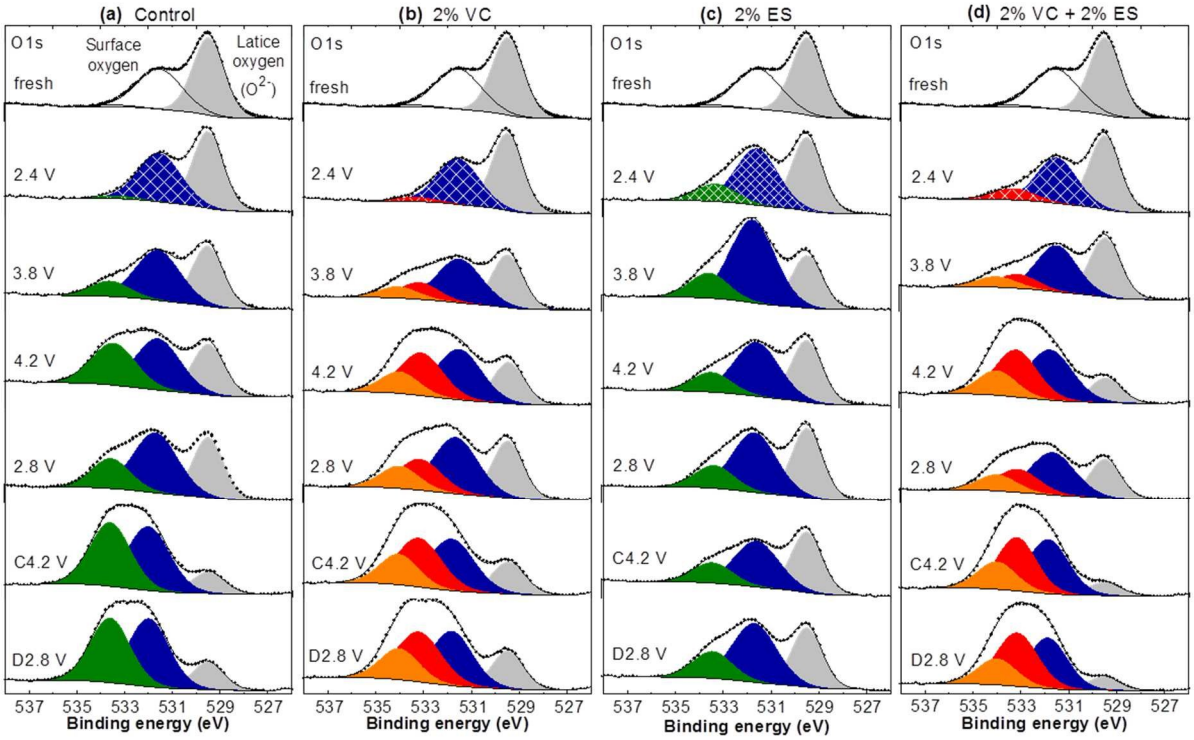

Figure 10. O 1s XPS core spectra for $LiNi_{1/3}Mn_{1/3}Co_{1/3}O_2$ electrodes with (a) control, (b) 2% VC, (c) 2% ES, and (d) 2% VC + 2% ES electrolytes taken from cells during formation at 2.4 V, 3.8 V and 4.2 V during charge and 2.8 V during discharge as well as after cycling at 4.2 V during charge (C4.2 V) and at 2.8 V during discharge (D2.8 V) at C/20 and 40. ± 0.1°C.

3.4.3 Further Studies on F-, P-, and S-containing Species. This section shows the analysis of the F 1s, P 2p and S 2p XPS core spectra for both graphite and NMC electrodes. The exact F 1s and P 2p core component assignments can be found in details

in our previous work.[24] The atomic percentage (at. %) of the F 1s peak associated to LiF for both graphite and NMC electrodes is presented in Table 2. The amount of LiF increased during the first charge then decreased during discharge while the SEI thickness decreased which suggests that LiF is formed throughout the entire SEI thickness. This phenomenon was still observed after cycling for graphite electrodes. LiF is therefore more likely formed via an electrochemical reduction of the PF_6^- anion during charge rather than via an impurity from hydrolysis. Also, the LiF content was 2 - 5 times higher at the graphite surface (Table 2), as expected if mostly formed by reduction. This result is in agreement with the higher amount of phosphates (P_xO_y) and fluorophosphate ($Li_xPO_yF_z$) compounds found at the surface of graphite electrodes (Tables S2 and S3). Also, the amount of P_xO_y was higher than the amount of $Li_xPO_yF_z$ at the graphite surface and inversely for NMC electrodes highlighting a different reactivity of the $LiPF_6$ salt at the graphite and NMC surfaces.

For VC-containing electrolytes, the overall evolution of the LiF content (Table 2) and the P_xO_y / $Li_xPO_yF_z$ content (Tables S2 and S3) was similar compared to control electrolyte. This result means that VC has no beneficial impact on the degradation of $LiPF_6$. Cells with 2% ES showed, however, less LiF, phosphates and fluorophosphates at the graphite surface (Tables 2, S2 and S3) compared to control electrolyte except at 2.4 V. At this voltage, much higher contents were observed more likely due to the vigorous reactivity of ES. At the NMC surface, the apparent increase amount of LiF, P_xO_y and $Li_xPO_yF_z$ for ES alone is more likely virtual as almost no organic compounds from solvent degradation were observed in the C 1s and O 1s core spectra of NMC electrodes (Figures 9 and 10). The use of ES therefore leads to a more inorganic SEI film at the NMC surface. Note that although a very thin SEI film was found at the NMC surface with 2% ES electrolyte (Figures 9 and 10), the more inorganic nature of this film may explain the much larger impedance measured by symmetric cells made from NMC/graphite pouch cells compared to control and 2% VC electrolytes.[40]

Figure 11 shows the evolution of the S content for both graphite and NMC electrodes. At 2.4 V, both ES-containing electrolytes showed a 2.5 times higher S content at the NMC surface compared to the graphite surface. Moreover, at 2.4 V, cells with 2% ES showed a 5.5 times higher S content at both the graphite and NMC surface compared to cells with 2% VC + 2% ES (Figure 11), in good agreement with the ~ 6 times higher total consumption of ES observed by GC-MS (Figure 3b). After formation at 3.8 V, the much larger S content for 2% ES was still observed in agreement with the GC-MS results (Figure 3b). During further formation and cycling, the S content for 2% ES electrolyte increased/decreased with time at the surface of the graphite/NMC electrodes, respectively. As almost all the ES molecules have initially reacted after the formation at 3.5 V (Figure 3b), this opposite evolution of the S content may indicate a migration of S species from the NMC to the graphite surface during cycling due to the absence of an efficient passivating film at the NMC surface when ES was used alone. When VC was added to ES, the S content continuously increased during formation and cycling at both the graphite and NMC surfaces. This result means that for 2% VC + 2% ES electrolyte, the initial reaction of ES is slow in agreement with the low consumption of ES (Figure 3b) and that ES continues to react slowly during cycling due to the dominant/passivating role of VC at the surface of both graphite and NMC electrodes.

Table 3. Atomic percentage (at. %) of the F 1s peak associated with LiF as measured from the XPS quantification at the surface of graphite and NMC electrodes as function of the voltage of the cell during formation and after cycling.

Sample	Graphite						$LiNi_{1/3}Mn_{1/3}Co_{1/3}O_2$					
	2.4V	3.8V	4.2V	2.8V	C4.2V	D2.8V	2.4V	3.8V	4.2V	2.8V	C4.2V	D2.8V
Control	1.1	15.4	16.3	12.3	11.6	9.2	1.4	1.3	2.5	2.0	2.6	2.8
2% VC	2.5	5.4	6.0	5.4	12.8	12. 3	2.1	2.2	4.8	1.9	2.4	3.5
2% ES	8.1	7.4	8.1	5.6	6.8	2.8	5.1	6.7	7.5	5.5	5.7	5.2
2% VC + 2% ES	4.7	6.3	11.0	5.4	13.3	14.0	1.4	1.9	5.7	2.5	4.5	5.2

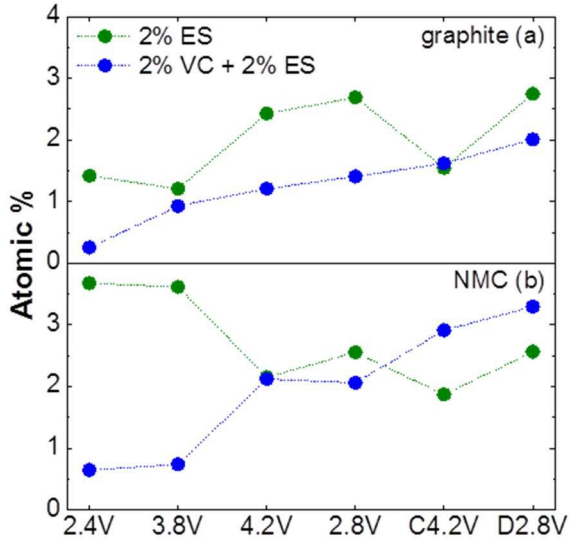

Figure 11. Evolution of the S content at the surface of both graphite and $LiNi_{1/3}Mn_{1/3}Co_{1/3}O_2$ electrodes cycled at 40°C for 2% ES and 2% VC + 2% ES electrolytes as determined from XPS quantification.

Figure 12 shows the S 2p core spectra of both graphite and NMC electrodes from cells with 2% ES compared to 2% VC + 2% ES electrolytes during formation and after 24 cycles. The S 2p core spectra of graphite electrode showed five components at 169.2, 167.0, 163.6, 161.6, 160.2 eV. The peaks at 169.2 and 167.1 eV can be attributed to sulfite species (RSO_3) such as $ROSO_2Li$ and Li_2SO_3, respectively.[39] The peak at 163.6 eV can be assigned to either $RSSO_3$ such as $Li_2S_2O_3$[74] and/or S-like[39] species while the two components at very low binding energy (161.6, 160.3 eV) are both assigned to Li_2S.[39,74] The S 2p core spectra of NMC electrodes showed three components at 168.6, 166.2, 163.8 eV. No formation of Li_2S was therefore observed at the NMC surface as expected. Moreover, considering the relatively small binding energy difference of the S 2p peaks for NMC electrodes compared to the graphite, it is more likely that the three peaks arise from similar species.

For graphite electrodes (Figure 12a and b), both ES-containing electrolytes showed similar contribution of the S 2p peaks until formation at 3.8 V. During formation at 4.2 V, 2% ES electrolyte (Figure 12a) showed a significant increase of the two main S 2p components at 169.2 eV ($ROSO_2Li$) and 163.6 eV ($RSSO_3$ and/or S-like species) which explains the increase of the S content at the graphite surface (Figure 11a). After cycling, the peak at 169.2 eV decreased to the benefit of the peak at 163.6 eV. Also, the huge increase of the 163.6 eV peak intensity observed during discharge correlates well with the increase of S content (Figure 11a) and indicates a relatively poor stability of the corresponding $RSSO_3$ and/or S-like species. When VC was added to ES, an opposite evolution was observed (Figure 12b). Also, the peak at 167.0 eV on the graphite electrode (Li_2SO_3) was much more intense with the addition of VC to ES and it increased with cycling (Figure 12b). VC therefore significantly modifies the reactivity of ES at the graphite surface by favoring the formation of sulfite species (RSO_3). The addition of VC to ES, therefore greatly decreased the amount of reduced sulfur species at the graphite surface compared to ES alone in good agreement with a lower reactivity of ES.

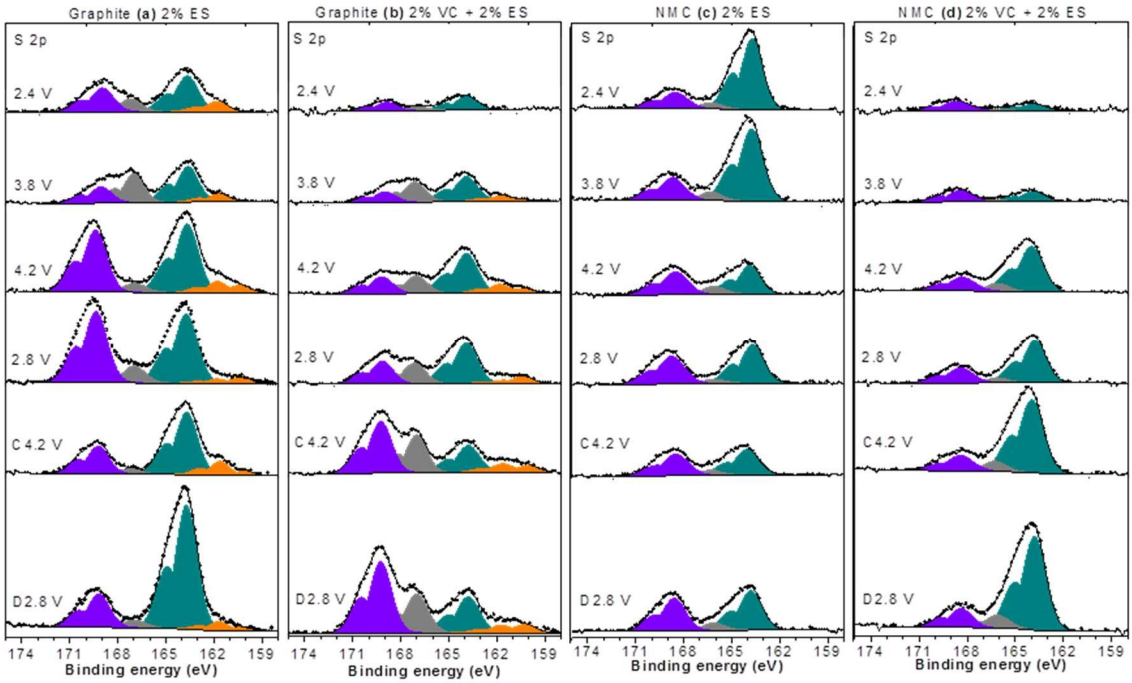

Figure 12. S 2p core spectra for graphite electrodes with (a) 2% ES and (b) 2% VC + 2% ES electrolytes as well as for $LiNi_{1/3}Mn_{1/3}Co_{1/3}O_2$ electrodes with (c) 2% ES and (d) 2% VC + 2% ES electrolytes taken from cells during formation at 2.4 V, 3.8 V and 4.2 V during charge and 2.8 V during discharge as well as after cycling at 4.2 V during charge (C4.2 V) and at 2.8 V during discharge (D2.8 V) at C/20 and 40. ± 0.1°C.

Journal Name

ARTICLE

For NMC electrodes, when ES was used, the peak at 163.8 eV ($RSSO_3$ and/or S-like species) showed a significant decrease after formation at 4.2 V (Figure 12c) which corresponds to the large decrease of S content observed previously (Figure 11b). This result indicates again a relatively poor stability of the corresponding species. It is believed that the corresponding species migrate to the negative electrode where they are deposited with time which would partially explain the relative increase of the 163.6 eV component at the graphite surface after cycling. When VC was added to ES (Figure 12d), similarly to the graphite electrode, no significant change was observed before 4.2 V where the peak at 163.8 eV increased. After cycling, a further increase of this peak was observed corresponding to the increase of S content observed at the NMC surface (Figure 11b). The species corresponding to the 163.8 eV component appears therefore more stable when VC is combined with ES. 2% VC + 2% ES electrolyte showed therefore an opposite evolution of the sulfur species at the NMC surface compared to the graphite surface. A migration of sulfur species from one electrode to the other is then unlikely in this case which indicates the formation of more stable SEI films at the surface of both graphite and NMC electrodes when both VC and ES are used.

3.4.4 Summary of the XPS data. Figure 13 shows schematic representations of the SEI films highlighting the differences between the graphite and NMC SEI films as observed from the XPS data. Figure 9 focuses on the results obtained during formation and after cycling at 4.2 V during charge. The heights of the SEI films in Figure 13 are proportional to their estimated heights, except for two cases where the thickness is so great the underlying graphite feature at about 282.5 eV cannot be observed. For instance, SEI thicknesses were estimated to be about 12 nanometers at the graphite surface and 2 nanometers at the NMC surface for control electrolyte during formation at 4.2 V (see experimental section for details). In each panel of Figure 13, the distribution of the species is based on the evolution of their content between the different states of charge while the number of times a species appears and the font size are proportional to the relative amount of the associated core level peak in atomic percentage (at. %) as measured from the XPS quantification. For instance, at the graphite surface during formation at 4.2 V, electrodes with control electrolyte showed about 44 at. % of fluorine from LiF, 30 at. % of oxygen from $-CO_2$ ($ROCO_2Li$), 12 at. % of oxygen from -C-O-, 5 at. % of oxygen from Li_2O and 9 at. % of phosphorus from P_xO_y, $Li_xPO_yF_z$ and Li_xPF_y. The sum of the different species in one panel is equal to 100 % which allows a direct comparison between samples.

At the graphite surface, at 4.2 V during formation, electrodes with control electrolyte showed a large fraction of inorganic compounds, mostly LiF and some Li_2O, as well as organic species like alkyl carbonates ($ROCO_2Li$) formed by the degradation of both $LiPF_6$ salt and the solvent (EC and/or EMC). After cycling, electrodes tested in control electrolyte showed a more organic concentration in the outermost SEI and the presence of Li_2O due to an unstable SEI film that led to the continuous degradation of the solvents and a relatively thick SEI film. When VC was used alone, a thinner and more organic SEI film was initially formed at the graphite surface due to the formation of Oligo-VC. After cycling, almost no change of SEI thickness and composition was observed for 2% VC electrolyte compared to control cells due to the formation of a more stable and passivating SEI film at the graphite surface. For ES alone, a thinner and more organic SEI film was initially formed at the graphite surface due to the contribution of sulfur species (RSO_x with x = 0 or 3). However, despite a very similar SEI composition, the use of ES alone led to a large increase of the SEI thickness after cycling indicating a less passivating role of ES compared to VC. When VC was combined with ES, similar SEI thicknesses were observed during formation and cycling compared to VC alone indicating the dominant role of VC on the SEI film formation.

At the NMC surface, thinner and more organic SEI films were observed for all electrolytes compared to those found at the graphite surface. NMC electrodes tested with control electrolyte showed larger relative amounts of ether derivatives -C-O- and alkyl carbonates ($ROCO_2Li$) during both formation and after cycling. NMC electrodes tested with control electrolyte also showed the larger SEI thickness increase at the NMC surface after cycling due to a poorly-passivating SEI film. For NMC electrodes tested with VC alone, a thicker SEI was found during formation and almost no change was observed after cycling indicating a stable and more passivating SEI film at the NMC surface due to Oligo-VC. For ES alone, very thin and inorganic SEI films were observed at the NMC surface during both formation and cycling with the presence of sulfur species (RSO_x with x = 0 or 3) which may indicate the formation of an unstable and poorly passivating SEI film at the NMC surface. When VC was combined with ES, thicker SEI films were found compared to ES alone indicating the dominant contribution of VC on the SEI film formation.

Journal Name

ARTICLE

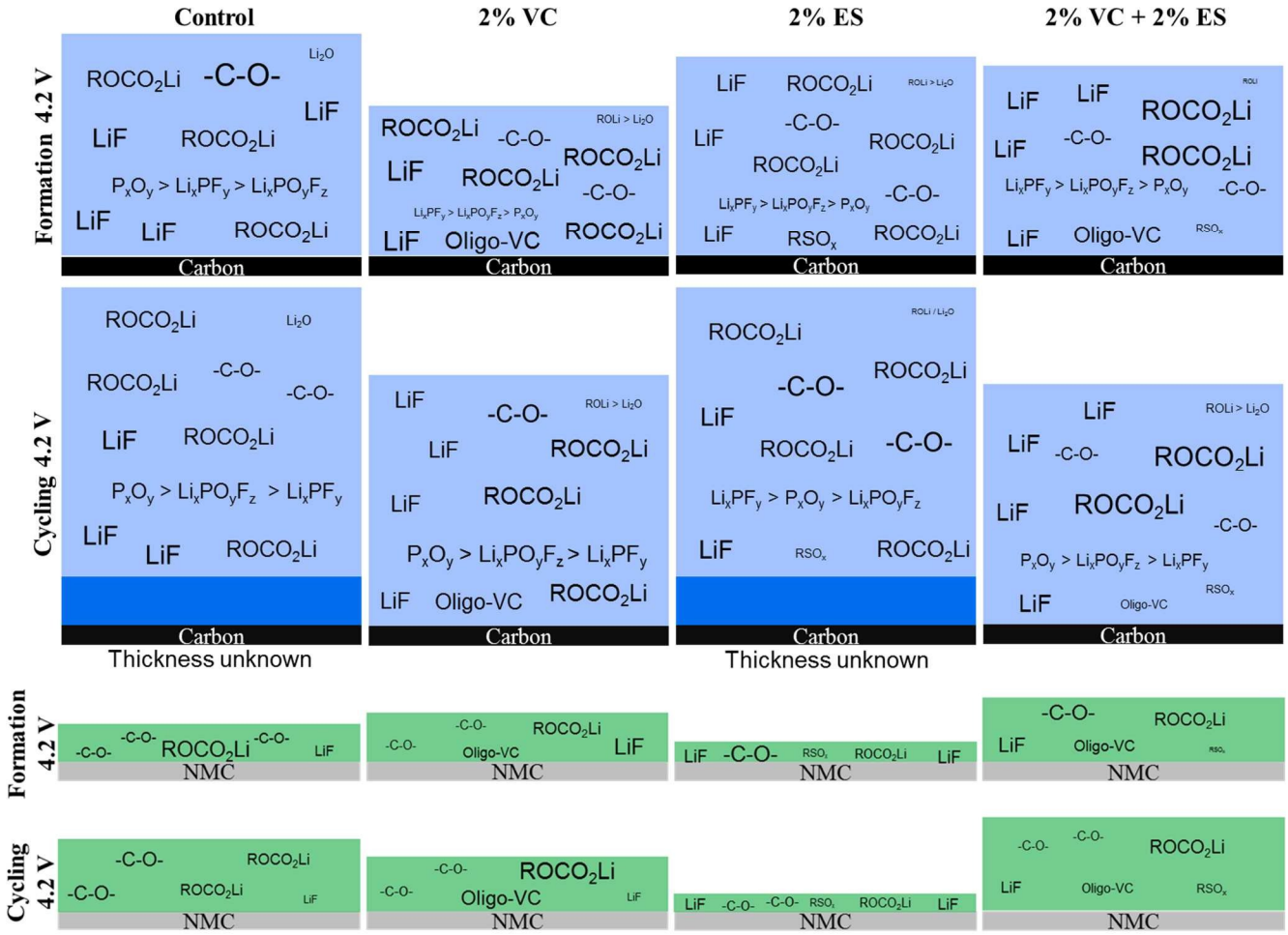

Figure 13. Schematic representations of the SEI films on the lithiated graphite and delithiated NMC electrodes taken from NMC/graphite pouch cells during formation and after cycling at 4.2 V for the different electrolytes, as deduced from the XPS experiments. The heights of the SEI films in Figure 13 are proportional to their estimated heights, except for two cases where the thickness is so great the underlying graphite feature at about 282.5 eV cannot be observed. For NMC electrodes, small amounts of Li_xPF_y, $Li_xPO_yF_z$ and P_xO_y (less than 5 at. % in total) were also found in the SEI films (see Table S3) but are not represented in the schematic diagrams for better clarity. For sulfur species (RSO_x), x = 0 or 3.

4. Conclusions

The role of ethylene sulfite used either alone or in combination with VC on the NMC/graphite pouch cells lifetime has been thoroughly investigated. Liquid GC−MS was used to precisely interpret the dQ/dV vs. V plots recorded during the early stages of the formation cycle. Theoretical calculations were used to understand the reactivity of ES and VC alone or in combination. ES had lowest reduction energy both with and without lithium leading to its vigorous reaction. A preferential solvation of Li+ by VC compared to ES was computationally found which explained why VC became more likely reduced when combined with ES. In situ gas volume analysis showed that the vigorous reaction of ES alone, which corresponded to a total of about 4-electrons per ES molecule, produced indirectly a very large amount of gas. When VC was added to ES, the properties of VC suppressed the vigorous reaction of ES and greatly reduced the gas generation. GC-MS analysis of the gaseous products formed during formation showed that the reaction of VC generated CO2 and greatly decreased the production of ethene from the reduction of EC. ES used alone produced similar gases as control electrolyte but with significantly higher amounts and additional gaseous products such as ethylene sulfide (C2H4S) or from side reactions involving the solvents. The larger production of gas with ES

was therefore attributed to both the vigorous reaction of ES and a larger reactivity of EC and EMC at the graphite surface. When VC was added to ES, the production of all additional gaseous compounds were suppressed and carbonyl sulfide (O=C=S) was found instead of the C2H4S observed for ES alone indicating again the dominant role of VC during the SEI formation process.

Ultrahigh precision coulometry and storage experiments were then correlated to thorough XPS analysis of the SEI films formed at both negative and positive electrodes during formation and after cycling. It was shown that VC formed a polymer (Oligo-VC) at the surface of both graphite and NMC electrodes. This resulted in more stable SEI films that greatly helped the prevention of parasitic reactions and explains the better CIE, charge end point capacity slippage, voltage drop during storage and capacity retention for long term cycling as well as the lower production of gas during cycling compared to control electrolyte. On the other hand, while ES alone formed an apparently stable and efficient SEI film at the graphite surface, it also formed a very thin, more inorganic and inefficient SEI film at the NMC surface compared to the other electrolytes. This was found to be the main reason for the dramatic decrease of the electrochemical performance as well as the continuous production of gas during cycling observed when ES was used alone. When VC was combined with ES, however, similar but slightly less stable SEI films were found compared to VC electrolyte which explains why the combination of VC with ES competed with VC alone. The study of the S 2p core spectra confirmed the higher reactivity of ES alone which reacts fully during formation compared to a slow and continuous reaction of ES when VC was added. It also showed that ES alone leads to the formation of less stable sulfur species and that when VC was added different and more stables species were found due to the dominant/passivating role of VC at the surface of both graphite and NMC electrodes.

Acknowledgements

The authors acknowledge financial support of this work by 3M Canada and NSERC under the auspices of the Industrial Chairs Program. Support from NSERC Automotive Partnership is also gratefully acknowledged. Remi Petibon thanks NSERC and the Walter C. Sumner Foundation for Scholarship support. The authors thank Dr. Jing Li of BASF for providing many of the electrolyte components used in this work.

References

1 E. Peled, *J. Electrochem. Soc.*, 1979, **126**, 2047–2051.
2 S. S. Zhang, *J. Power Sources*, 2006, **162**, 1379–1394.
3 K. Xu, *Chem. Rev.*, 2004, **104**, 4303–4418.
4 X. Zhang, R. Kostecki, T. J. Richardson, J. K. Pugh and P. N. Ross, *J. Electrochem. Soc.*, 2001, **148**, A1341–A1345.
5 D. Aurbach, K. Gamolsky, B. Markovsky, Y. Gofer, M. Schmidt and U. Heider, *Electrochimica Acta*, 2002, **47**, 1423–1439.
6 R. Mogi, M. Inaba, S.-K. Jeong, Y. Iriyama, T. Abe and Z. Ogumi, *J. Electrochem. Soc.*, 2002, **149**, A1578–A1583.
7 H. Ota, K. Shima, M. Ue and J. Yamaki, *Electrochimica Acta*, 2004, **49**, 565–572.
8. B. Simon, J.-P. Boeuve, U.S. Patent 5,626,981, 1997.
9 M. Contestabile, M. Morselli, R. Paraventi and R. J. Neat, *J. Power Sources*, 2003, **119–121**, 943–947.
10 M. Holzapfel, C. Jost, A. Prodi-Schwab, F. Krumeich, A. Würsig, H. Buqa and P. Novák, *Carbon*, 2005, **43**, 1488–1498.
11 T. Sasaki, T. Abe, Y. Iriyama, M. Inaba and Z. Ogumi, *J. Electrochem. Soc.*, 2005, **152**, A2046–A2050.
12 E.-G. Shim, T.-H. Nam, J.-G. Kim, H.-S. Kim and S.-I. Moon, *J. Power Sources*, 2007, **172**, 901–907.
13 L. Chen, K. Wang, X. Xie and J. Xie, *J. Power Sources*, 2007, **174**, 538–543.
14 J. C. Burns, G. Jain, A. J. Smith, K. W. Eberman, E. Scott, J. P. Gardner and J. R. Dahn, *J. Electrochem. Soc.*, 2011, **158**, A255–A261.
15 N. N. Sinha, A. J. Smith, J. C. Burns, G. Jain, K. W. Eberman, E. Scott, J. P. Gardner and J. R. Dahn, *J. Electrochem. Soc.*, 2011, **158**, A1194–A1201.
16 R. Petibon, E. C. Henry, J. C. Burns, N. N. Sinha and J. R. Dahn, *J. Electrochem. Soc.*, 2014, **161**, A66–A74.
17 J. C. Burns, R. Petibon, K. J. Nelson, N. N. Sinha, A. Kassam, B. M. Way and J. R. Dahn, *J. Electrochem. Soc.*, 2013, **160**, A1668–A1674.
18 J. Jeon, S. Yoon, T. Park, J.-J. Cho, S. Kang, Y.-K. Han and H. Lee, *J. Mater. Chem.*, 2012, **22**, 21003–21008.
19 H. M. Jung, S.-H. Park, J. Jeon, Y. Choi, S. Yoon, J.-J. Cho, S. Oh, S. Kang, Y.-K. Han and H. Lee, *J. Mater. Chem. A*, 2013, **1**, 11975–11981.
20 H. Ota, Y. Sakata, A. Inoue and S. Yamaguchi, *J. Electrochem. Soc.*, 2004, **151**, A1659–A1669.
21 Y. Wang, S. Nakamura, K. Tasaki and P. B. Balbuena, *J. Am. Chem. Soc.*, 2002, **124**, 4408–4421.
22 L. E. Ouatani, R. Dedryvère, C. Siret, P. Biensan, S. Reynaud, P. Iratçabal and D. Gonbeau, *J. Electrochem. Soc.*, 2009, **156**, A103–A113.
23 L. E. Ouatani, R. Dedryvère, C. Siret, P. Biensan and D. Gonbeau, *J. Electrochem. Soc.*, 2009, **156**, A468–A477.
24 L. Madec, J. Xia, R. Petibon, K. J. Nelson, J.-P. Sun, I. G. Hill and J. R. Dahn, *J. Phys. Chem. C*, 2014.
25 X. Zuo, C. Fan, X. Xiao, J. Liu and J. Nan, *ECS Electrochem. Lett.*, 2012, **1**, A50–A53.
26 J. Xia, N. N. Sinha, L. P. Chen, G. Y. Kim, D. J. Xiong and J. R. Dahn, *J. Electrochem. Soc.*, 2014, **161**, A84–A88.
27 J. Xia, N. N. Sinha, L. P. Chen and J. R. Dahn, *J. Electrochem. Soc.*, 2014, **161**, A264–A274.
28 J. Xia, J. E. Harlow, R. Petibon, J. C. Burns, L. P. Chen and J. R. Dahn, *J. Electrochem. Soc.*, 2014, **161**, A547–A553.
29 P. Janssen, R. Schmitz, R. Müller, P. Isken, A. Lex-Balducci, C. Schreiner, M. Winter, I. Cekić-Lasković and R. Schmitz, *Electrochimica Acta*, 2014, **125**, 101–106.
30 S.-K. Jeong, M. Inaba, R. Mogi, Y. Iriyama, T. Abe and Z. Ogumi, *Langmuir*, 2001, **17**, 8281–8286.
31 G. H. Wrodnigg, J. O. Besenhard and M. Winter, *J. Electrochem. Soc.*, 1999, **146**, 470–472.
32 G. H. Wrodnigg, J. O. Besenhard and M. Winter, *J. Power Sources*, 2001, **97–98**, 592–594.
33 A. Sano and S. Maruyama, *J. Power Sources*, 2009, **192**, 714–718.
34 M. Xu, W. Li and B. L. Lucht, *J. Power Sources*, 2009, **193**, 804–809.

35 K. Abe, H. Yoshitake, T. Kitakura, T. Hattori, H. Wang and M. Yoshio, *Electrochimica Acta*, 2004, **49**, 4613–4622.
36 L. Xing, W. Li, M. Xu, T. Li and L. Zhou, *J. Power Sources*, 2011, **196**, 7044–7047.
37 E. G. Leggesse and J.-C. Jiang, *J. Phys. Chem. A*, 2012, **116**, 11025–11033.
38 M. D. Bhatt and C. O'Dwyer, *J. Electrochem. Soc.*, 2014, **161**, A1415–A1421.
39 H. Ota, T. Akai, H. Namita, S. Yamaguchi and M. Nomura, *J. Power Sources*, 2003, **119–121**, 567–571.
40 J. Xia, C. P. Aiken, L. Ma, G. Y. Kim, J. C. Burns, L. P. Chen and J. R. Dahn, *J. Electrochem. Soc.*, 2014, **161**, A1149–A1157.
41 A. J. Smith, J. C. Burns, S. Trussler and J. R. Dahn, *J. Electrochem. Soc.*, 2010, **157**, A196–A202.
42 T. M. Bond, J. C. Burns, D. A. Stevens, H. M. Dahn and J. R. Dahn, *J. Electrochem. Soc.*, 2013, **160**, A521–A527.
43 R. Petibon, L. M. Rotermund and J. R. Dahn, *J. Power Sources*, 2015, **287**, 184–195.
44 S. Tanuma, C. J. Powell and D. R. Penn, *Surf. Interface Anal.*, 1994, **21**, 165–176.
45 S. Tanuma, C. J. Powell and D. R. Penn, *Surf. Interface Anal.*, 1991, **17**, 927–939.
46 G. V. Zhuang, K. Xu, H. Yang, T. R. Jow and P. N. Ross, *J. Phys. Chem. B*, 2005, **109**, 17567–17573.
47 K. Xu, Y. Lam, S. S. Zhang, T. R. Jow and T. B. Curtis, *J. Phys. Chem. C*, 2007, **111**, 7411–7421.
48 R. Petibon, L. Rotermund, K. J. Nelson, A. S. Gozdz, J. Xia and J. R. Dahn, *J. Electrochem. Soc.*, 2014, **161**, A1167–A1172.
49 J.-Y. Eom, I.-H. Jung and J.-H. Lee, *J. Power Sources*, 2011, **196**, 9810–9814.
50 S. E. Sloop, J. B. Kerr and K. Kinoshita, *J. Power Sources*, 2003, **119–121**, 330–337.
51 H. Yoshida, T. Fukunaga, T. Hazama, M. Terasaki, M. Mizutani and M. Yamachi, *J. Power Sources*, 1997, **68**, 311–315.
52 T. Sasaki, T. Abe, Y. Iriyama, M. Inaba and Z. Ogumi, *J. Power Sources*, 2005, **150**, 208–215.
53 H. Kim, S. Grugeon, G. Gachot, M. Armand, L. Sannier and S. Laruelle, *Electrochimica Acta*, 2014, **136**, 157–165.
54 J. Self, C. P. Aiken, R. Petibon and J. R. Dahn, *J. Electrochem. Soc.*, 2015, **162**, A796–A802.
55 W. Kong, H. Li, X. Huang and L. Chen, *J. Power Sources*, 2005, **142**, 285–291.
56 M. Onuki, S. Kinoshita, Y. Sakata, M. Yanagidate, Y. Otake, M. Ue and M. Deguchi, *J. Electrochem. Soc.*, 2008, **155**, A794–A797.
57 I. A. Shkrob, Y. Zhu, T. W. Marin and D. Abraham, *J. Phys. Chem. C*, 2013, **117**, 19255–19269.
58 R. Mogi, M. Inaba, Y. Iriyama, T. Abe and Z. Ogumi, *J. Power Sources*, 2003, **119–121**, 597–603.
59 J. C. Burns, N. N. Sinha, G. Jain, H. Ye, C. M. VanElzen, W. M. Lamanna, A. Xiao, E. Scott, J. Choi and J. R. Dahn, *J. Electrochem. Soc.*, 2012, **159**, A1105–A1113.
60 D. Pantea, H. Darmstadt, S. Kaliaguine, L. Sümmchen and C. Roy, *Carbon*, 2001, **39**, 1147–1158.
61 D. Pantea, H. Darmstadt, S. Kaliaguine and C. Roy, *Appl. Surf. Sci.*, 2003, **217**, 181–193.
62 D. Aurbach, M. L. Daroux, P. W. Faguy and E. Yeager, *J. Electrochem. Soc.*, 1987, **134**, 1611–1620.
63 M. Nie, D. Chalasani, D. P. Abraham, Y. Chen, A. Bose and B. L. Lucht, *J. Phys. Chem. C*, 2013, **117**, 1257–1267.
64 S. Malmgren, K. Ciosek, M. Hahlin, T. Gustafsson, M. Gorgoi, H. Rensmo and K. Edström, *Electrochimica Acta*, 2013, **97**, 23–32.
65 R. Dedryvère, L. Gireaud, S. Grugeon, S. Laruelle, J.-M. Tarascon and D. Gonbeau, *J. Phys. Chem. B*, 2005, **109**, 15868–15875.
66 Q. Wang, J. Sun, X. Yao and C. Chen, *Thermochim. Acta*, 2005, **437**, 12–16.
67 G. Gachot, S. Grugeon, M. Armand, S. Pilard, P. Guenot, J.-M. Tarascon and S. Laruelle, *J. Power Sources*, 2008, **178**, 409–421.
68 I. Ismail, A. Noda, A. Nishimoto and M. Watanabe, *Electrochimica Acta*, 2001, **46**, 1595–1603.
69 L. J. Rendek, G. S. Chottiner and D. A. Scherson, *J. Electrochem. Soc.*, 2002, **149**, E408–E412.
70 S.-P. Kim, A. C. T. van Duin and V. B. Shenoy, *J. Power Sources*, 2011, **196**, 8590–8597.
71 R. Dedryvère, D. Foix, S. Franger, S. Patoux, L. Daniel and D. Gonbeau, *J. Phys. Chem. C*, 2010, **114**, 10999–11008.
72 R. Petibon, C. P. Aiken, N. N. Sinha, J. C. Burns, H. Ye, C. M. VanElzen, G. Jain, S. Trussler and J. R. Dahn, *J. Electrochem. Soc.*, 2013, **160**, A117–A124.
73 R. Petibon, N. N. Sinha, J. C. Burns, C. P. Aiken, H. Ye, C. M. VanElzen, G. Jain, S. Trussler and J. R. Dahn, *J. Power Sources*, 2014, **251**, 187–194.
74 S. Xiong, K. Xie, Y. Diao and X. Hong, *J. Power Sources*, 2014, **246**, 840–845.